Design of a targeting and oxygen-independent platform to improve photodynamic therapy: A proof of concept

Ludivine Larue, Tataye Moussounda Moussounda Koumba, Nolwenn Le Breton, Bertrand Vileno, Philippe Arnoux, Valérie Jouan-Hureaux, Cédric Boura, Gerard Audran, Raphael Bikanga, Sylvain Marque, et al.

Design of a targeting and Oxygen-independent platform to improve Photodynamic Therapy: A proof of concept

Ludivine Larue,†, ‡ Tataye MOUSSOUNDA MOUSSOUNDA KOUMBA,♢ Nolwenn Le Breton,°,‖ Bertrand Vileno,°,‖ Philippe Arnoux,† Valérie Jouan-Hureaux,⊥ Cédric Boura,⊥ Gérard Audran,♢,* Raphael Bikanga,§ Sylvain R. A. Marque,♢ Samir Acherar,‡ and Céline Frochot,†,*

† Université de Lorraine, CNRS, LRGP, F-54000 Nancy, France ; ludivine.larue@univ-lorraine.fr, philippe.arnoux@univ-lorraine.fr, celine.frochot@univ-lorraine.fr

‡ Université de Lorraine, CNRS, LCPM, F-54000 Nancy, France ; samir.acherar@univ-lorraine.fr

♢ Aix Marseille Univ, CNRS, ICR, UMR 7273, case 551, Avenue Escadrille Normandie-Niemen, 13397 Marseille Cedex 20, France; g.audran@univ-amu.fr, sylvain.marque@univ-amu.fr, tataye.mousskoumb@gmail.com

° Institut de Chimie, UMR 7177, CNRS, Université de Strasbourg, 4 rue Blaise Pascal, F-67000 Strasbourg, France; nlebreton@unistra.fr, vileno@unistra.fr

‖ French EPR Federation of Research, REseau NAtional de Rpe interDisciplinaire, RENARD, Fédération IR-RPE CNRS 3443, France

⊥ Université de Lorraine, CNRS, CRAN, F-54000 Nancy, France ; valerie.jouan-hureaux@univ-lorraine.fr, cedric.boura@univ-lorraine.fr

§ Laboratoire de Substances Naturelles et de Synthèse Organométalliques, Université des Sciences et Techniques de Masuku, B.P. 943, Franceville, Gabon ; brbikanga@hotmail.fr

* Correspondence: celine.frochot@univ-lorraine.fr; Tel.: +33-3-72-74-37-80; g.audran@univ-amu.fr; Tel.: +33-4-91-28-88-62

KEYWORDS: photodynamic therapy, hypoxia, targeting, neuropilin-1, peptide, alkoxyamine, hemolysis, spin trapping

ABSTRACT:

Photodynamic therapy (PDT) is a promising technique to treat different kinds of disease especially cancer. PDT requires three elements: molecular oxygen, a photo-activatable molecule called the photosensitizer (PS) and appropriate light. Under illumination, the PSs generate, in the presence of oxygen, the formation of reactive oxygen species including singlet oxygen, toxic, which then destroys the surrounding tissues. Even if PDT is used with success to treat actinic keratosis or prostate cancer for example, PDT suffers from two major drawbacks: the lack of selectivity of most of the PSs currently used clinically as well as the need for oxygen to be effective. To remedy the lack of selectivity, targeting the tumor neovessels is a promising approach to destroy the vascularization and cause asphyxia of the tumor. KDPPR peptide affinity for the NRP-1 receptor overexpressed on endothelial cells has already been proven. To compensate for the lack of oxygen, we focused on photoactivatable alkoxyamines, molecules capable of generating toxic radicals by light activation. In this paper we describe the synthesis of a multifunctional platform combining three units: a PS for an oxygen-dependent PDT, a peptide to target tumor neovessels and an alkoxyamine for an oxygen-independent activity. The synthesis of the compound was successfully carried out, the study of the photophysical properties showed that the PS retained its capacity to form singlet oxygen, the affinity tests confirmed the affinity of the compound for NRP-1. Thanks to the Electron Paramagnetic Resonance (EPR) spectroscopy, a technique of choice for radical investigation, the radicals generated by the illumination of the alkoxyamine could be detected. The proof of concept was thus successfully established.

INTRODUCTION

Photodynamic therapy (PDT) is applied to treat many diseases[1] such as age-related macular degeneration (AMD), actinic keratoses, Barrett's esophagus, prostate cancer.

PDT is a simple and efficient approach requiring three components to be effective: the light, the molecular oxygen (triplet oxygen $^3O_2$) and a photosensitizer (PS). All these components are non-toxic taken apart but taken together, they are able to destroy cells at a specific location. This modality of treatment requires the illumination of the PS by light. Thus, the PS moves from the ground state to singlet excited state (^{1}PS*). After intersystem-crossing a triplet excited state (^{3}PS*) is formed. ^{3}PS* reacts with surrounding molecular $^3O_2$ to generate radical oxygen species (ROS) by two main types of reactions: (i) type I which conducts at the generation of superoxide anion ($O_2^{\cdot-}$) and

hydroxyl radical (HO•) (ii) type II where ^{3}PS* transfers its energy to $^3O_2$ to produce reactive singlet oxygen ($^1O_2$).[1]

Although PDT presents many well-known advantages, we can report, as well as for radiotherapy, the requirement of $^3O_2$ to be efficient.[2] Indeed, the PDT leads to the consumption of $^3O_2$ inside the tumor and thus PDT-induced hypoxia as well as tumor pre-existing hypoxia limit its efficiency. To fight tumor hypoxia, six strategies from literature have been reported by us in a recent review[3]: (1) the use of $^3O_2$ cargo to directly supply additional $^3O_2$ inside the tumor (oxyhemoglobin, perfluorocarbon…), (2) the modification of tumor microenvironment (H_2O_2 decomposition, decrease of tumor $^3O_2$ consumption…), (3) the use of combined therapies to have an additional effect to PDT (chemo-PDT, PTT-PDT…), (4) the fractional PDT to regulate tumor $^3O_2$ consumption, (5) the hypoxia-dependent PDT by using hypoxia-activated compounds (azobenzene) and (6) hypoxia-independent PDT by using compounds which do not need $^3O_2$ to be cytotoxic (PDT type I, NO or $^1O_2$ donor and photoactivatable compounds). The use of photoactivatable compounds that do not require $^3O_2$ to be effective appeared to be particularly interesting.

Alkoxyamines (Alks), with $R_1R_2NO—R_3$ (R_1, R_2 and R_3 as alkyl chains) as general structure, are interesting molecules for therapeutic aspects. Indeed, as depicted in the Scheme 1, alks having weak energy bond of $NO—R_3$ could release two radical species: a stable nitroxide ($R_1R_2NO^•$) and a transient alkyl radical ($R_3^•$). Moreover, both radicals could be coupled together to reform an alk.[4] Thus, this radical reactivity of alks has been intensely investigated in NMP (Nitroxide Mediated Polymerization).[5] Several relationships were developed linking the rate constants of homolysis k_d to polarity, bulkiness, and stability parameters of both the nitroxide ($R_1R_2NO^•$) and alkyl fragments($R_3^•$).[6] In 2014, we reported a proof of concept for a new application of alks as theranostic agents against cell tumours.[7] Thus, the release radical as therapeutic agent triggered the apoptosis of cancer cells *in vitro* and the nitroxide as diagnostic probe in imaging by Overhauser MRI. Recently, we optimized the efficiency of these reactive species to destroy malignant cells *in vitro*[8] and reported *in vivo* experiments in mouse.[9]

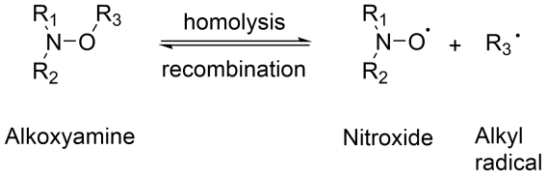

Scheme 1. Reversible $NO—R_3$ bond in alks.

Another limit of PDT is the low selectivity of the majority of the commercial PSs. The selectivity is therefore due to the possibility to confine the PS by restricting the light illumination to a specific region. However, this strategy is limited in some cases (spread metastases for example) needing a broader illumination. It is necessary to develop modified PSs able to target effectively the cancer cells by a specific accumulation into the tumor or the neovessels surrounding the tumor.[10] The destruction of the vascular system allows the eradication of the tumor, following the O_2 deprivation and nutrients essential to life.[11] Therefore, the tumor vascular system is a promising target for creating damage by PDT. Specific receptors of endothelial cells, such as vascular endothelial growth factor receptors (VEGF) or neuropilin-1 co-receptor (NRP-1) can be used as molecular targets.[12]

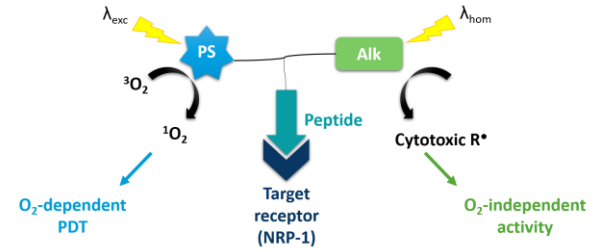

Figure 1. Schematic representation of trimodal platform.

Herein, we design trimodal platform for a targeted-PDT treatment efficient in both normoxic and hypoxic conditions. The designed platform, named Alk-K(Pyro-a)DKPPR, is based on three unities: (1) pyropheophorbide-a (**Pyro-a**) as a PS, which could be illuminated in the red region (Q_I = 668 nm) to have an O_2-dependent PDT, (2) KDKPPR, a NRP-1-targeted peptide has already been proven by our team and (3) a homolyzable alk, under UV illumination, to produce alkyl radicals in order to have an O_2-independent PDT (Figure 1). For the evaluation of the relevance of these new platforms, the synthesis of the following compounds is necessary: the bimodal platform without Alk (i.e. K(Pyro-a)DKPPR) on the one hand and the bimodal platform without **Pyro-a** (i.e. Alk-KDKPPR) on the other hand. In this study, we aim to establish the proof of concept that the combination of these three unities is possible without any disruption of their proper properties.

RESULTS AND DISCUSSION

Synthesis

Alk *(RS/SR)*-**6** was prepared in 4 steps in 37% overall yield. First, allylic bromination of 4-ethylbenzophenone **1** using *N*-bromosuccinimide (NBS) in CCl_4 afforded the bromide derivative *(R/S)*-**2** in 92 % yield (Scheme 2).[13] Then, the alkyl radical was generated *in situ* by the action of copper catalysts to the nitroxide *(R/S)*-**3**[14] with the bromide derivative yielded the alk **4** as a 4:1 mixture of diastereoisomers (55%).

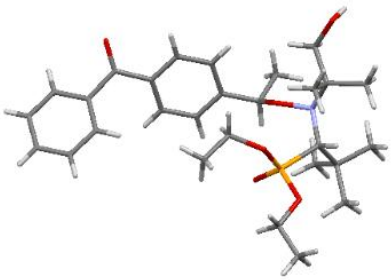

Figure 2. X-Ray structure of alk *(RS/SR)*-**4**.[15]

At this stage, the two diastereoisomers in racemic form were separated using column chromatography to afford 2.95 g of *(RS/SR)*-**4** and 0.80 g of *(RR/SS)*-**4**. Thanks to recrystallization of *(RS/SR)*-**4**[15] in diethyl ether white crystals suitable for X-ray analysis were obtained (Figure 2).

Finally, alk (*RS/SR*)-**6** was obtained through two successive oxidations with Dess–Martin periodinane (DMP)[16] and Pinnick oxidation procedure in 73% yield.[17]

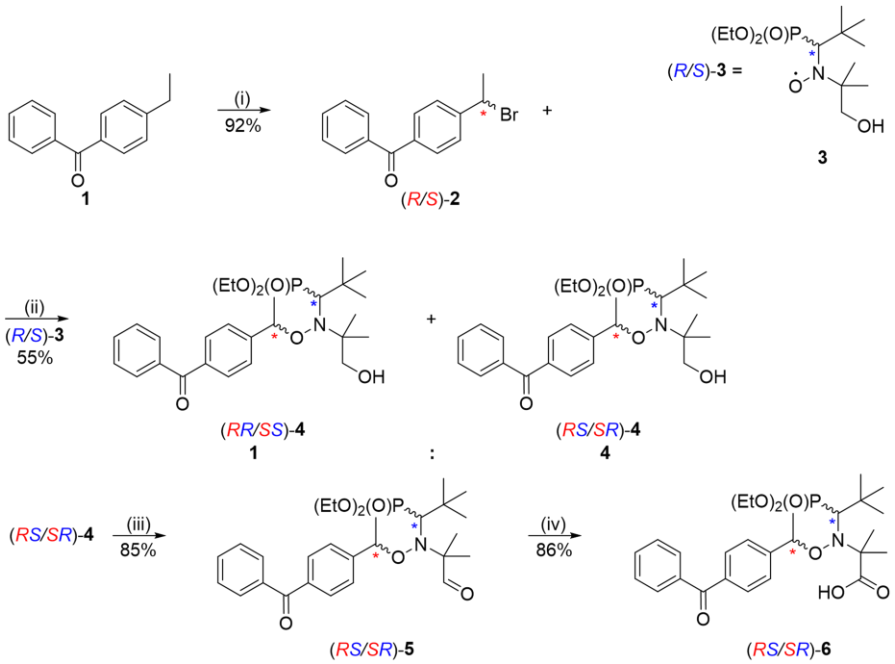

Scheme 2. Synthesis of alk *(RS/SR)*-6. (i) NBS, CCl_4, reflux, 5h, (ii) Cu/CuBr, rt, 12h, PMDTA, benzene, (iii) DMP, DCM, 0°C, 5h, and (iv) $NaClO_2$/NaH_2PO_4, *t*-BuOH, rt, 1.5h.

The amino acid lysine was chosen to link the three units (peptide, Alk and PS) together in our trimodal platform. First, the coupling reaction of the **Pyro-a** with the (ε)-amino group of lysine was done separately and performed in two steps in liquid phase to afford **Fmoc-K(Pyro-a)** as described previously by our team (Figure 3).[18]

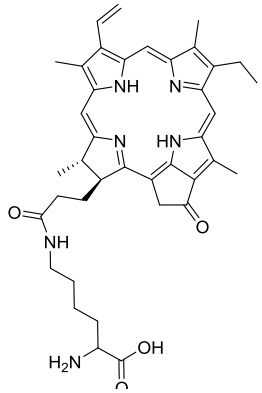

Figure 3. Structure of Fmoc-K(Pyro-a).

All the platforms, Alk-KDKPPR (**9**), K(Pyro-a)DKPPR (**12**) and Alk-K(Pyro-a)DKPPR (**13**) were prepared using a Fmoc/*t*Bu solid phase peptide synthesis (SPPS) on 4-benzyloxybenzyl alcohol (Wang) resin (Scheme 3) and characterized by HR-MS and ^{1}H NMR (See Supporting information). First, the peptide Fmoc-KDKPPR-wang resin **8** and Fmoc-DKPPR-wang resin **10** with protected lateral chains was synthesized. From these peptides, the bimodal platforms without Pyro-a (i.e. Alk-KDKPPR, **9**) and without Alk (i.e. K(Pyro-a)DKPPR, **12**), and the trimodal platform Alk-K(Pyro-a)DKPPR **13** were generated. The bimodal platform **9** was obtained after coupling reaction at the N-terminal extremity of peptide **8** with *(RS/SR)*-**6**, followed by both cleavages under acidic conditions (27% overall yield from **7** with a HPLC purity of 95%) of the peptide from the resin and of the lateral chains. The other bimodal platform **12** was isolated after a coupling reaction at the N-terminal extremity of peptide **10** with **Fmoc-K(Pyro a)** to afford **11**, then resin-cleaved and fully deprotected (25% overall yield from **7** with a HPLC purity of 100%). Finally, the trimodal platform **13** was obtained after similar procedure as **9** from **11** with *(RS/SR)*-**6**, (19% overall yield from **7** with a HPLC purity of 98%) (Figure 4).

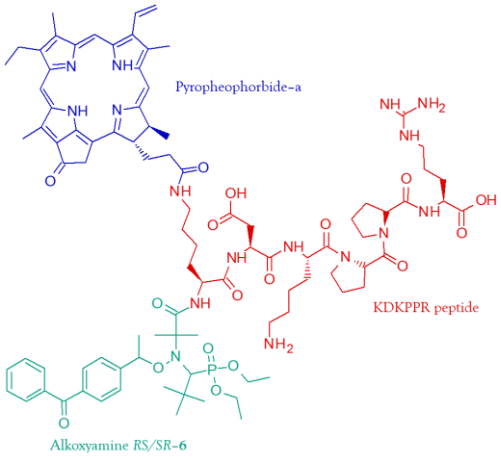

Figure 4. Structure of the trimodal platform **13**.

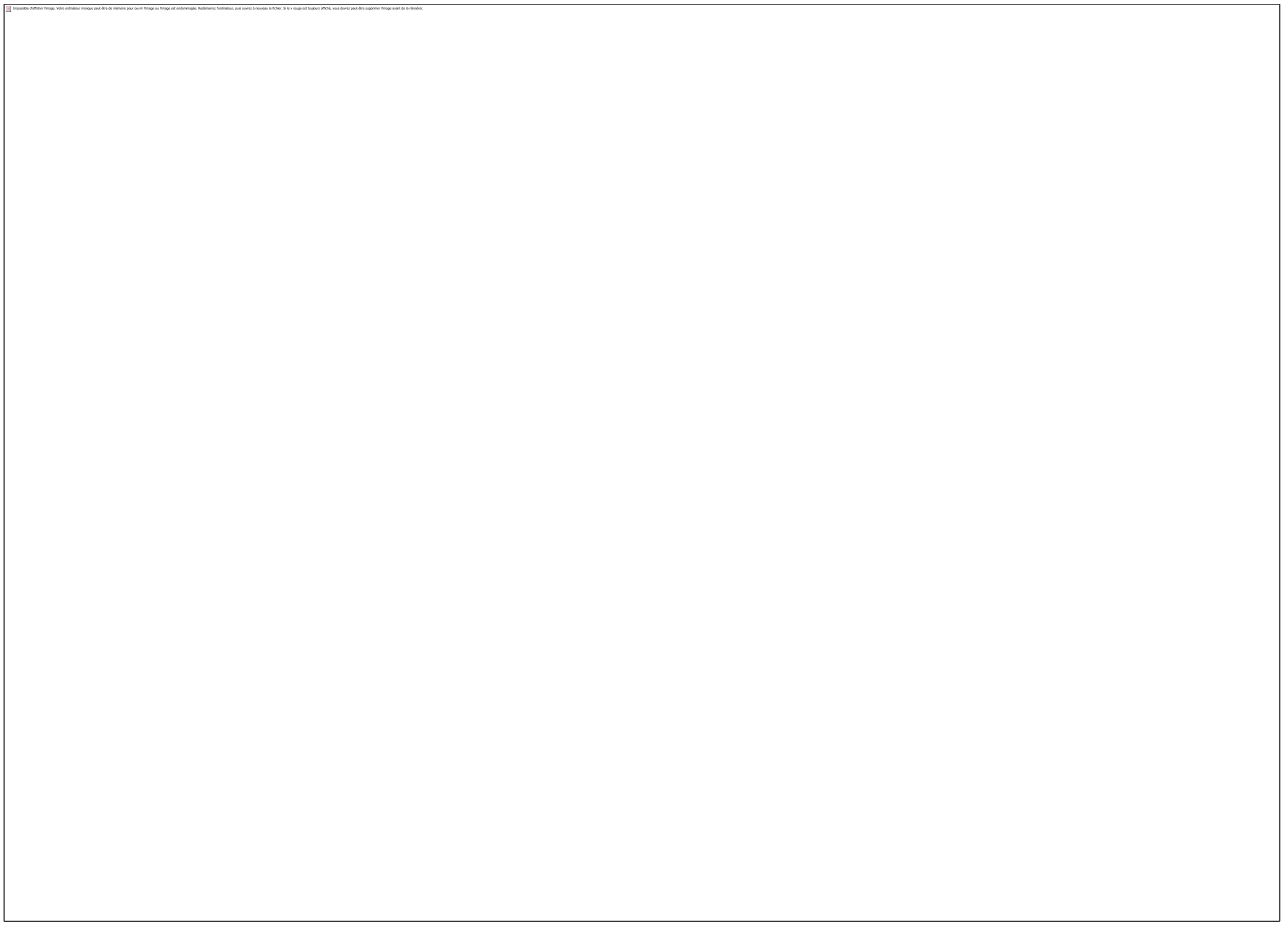

Scheme 3. Solid phase peptide synthesis of bimodal (9 and 12) and trimodal (13) platforms: (i) *N*-Deprotection: DMF/Pip (80:20, v:v), rt, 4 then 7 min (synthesizer) or 4x15 min (manually) (ii) Coupling: Fmoc-AA(P)-OH, HBTU, NMM, NMP, DMF, rt, 2 x 18 min, (iii) Coupling: PyBOP, DIPEA, DMF, rt, 12 h, (iv) Coupling: HBTU, NMM, NMP, DMF, rt, 12 h and (v) TFA/TIPS/water (92.5:2.5:5.0, v:v:v), rt, 1h30. Legend: *x*, number of amino acid.

Photophysical properties

The photophysical properties of the synthesized platforms (**9**, **12** and **13**) as well as those of *(RS/SR)*-**6** and **Pyro-a** alone were evaluated. These last two were used as references to test the influence of each moiety on the photophysical properties of **Pyro-a**. The photophysical studies were performed in methanol in which all the compounds were soluble. The absorption spectra of each compound were recorded at several concentrations to determine the ε values (Figure 5A). A slight decreased of the ε of **Pyro-a** was observed for the Soret and Q_I bands after conjugation with the peptide and alk moieties, but it remained high for PDT applications.

The absorption spectrum showed the typical absorption bands of **Pyro-a** at 410 (Soret band), 508 (Q_{IV}), 539 (Q_{III}), 609 (Q_{II}) and 666 (Q_I) nm. Moreover, the coupling of the peptide and alk led to the apparition of a band at 214 and 270 nm, respectively (Figure 5B).

Solutions of **Pyro-a**, (*RS/SR)*-**6**, **9**, **12** and **13** were prepared at a concentration allowing an absorbance of about 0.2. The fluorescence spectra were performed at an excitation wavelength at 410 nm for compounds containing **Pyro-a** (Figure 5C) and at 280 nm for compounds containing *(RS/SR)*-**6** (data not shown). The fluorescence quantum yields, Φ_f, could then be calculated (Figure 5A). No fluorescence was observed for compounds that do not contain **Pyro-a** (i.e. *(RS/SR)*-**6** and **9**). The $^1O_2$ emission spectra were carried out under the same conditions in order to determine the quantum yield of $^1O_2$, Φ_Δ (Figure 5A and Figure 5D).

As for the fluorescence, no $^1O_2$ production was highlighted for compounds *(RS/SR)*-**6** and **9**. It could be observed that there was a slight decrease of both quantum yields for **12** in comparison with **Pyro-a**. Moreover, for **13**, no change was observed. These results indicated that alk and peptide were not found to affect the photophysical properties of **Pyro-a**.

(A)

		Pyro-a	12	13
ε (10^3) ($L.mol^{-1}.cm^{-1}$)	Soret Band	91.1	64.1	51.8
	Q_{IV}	9.8	6.5	5.3
	Q_{III}	8.9	6.0	5.1
	Q_{II}	8.5	5.6	5.1
	Q_I	42.8	27.9	23.7
Φ_f (%)		34	28	32
Φ_Δ (%)		54	50	54

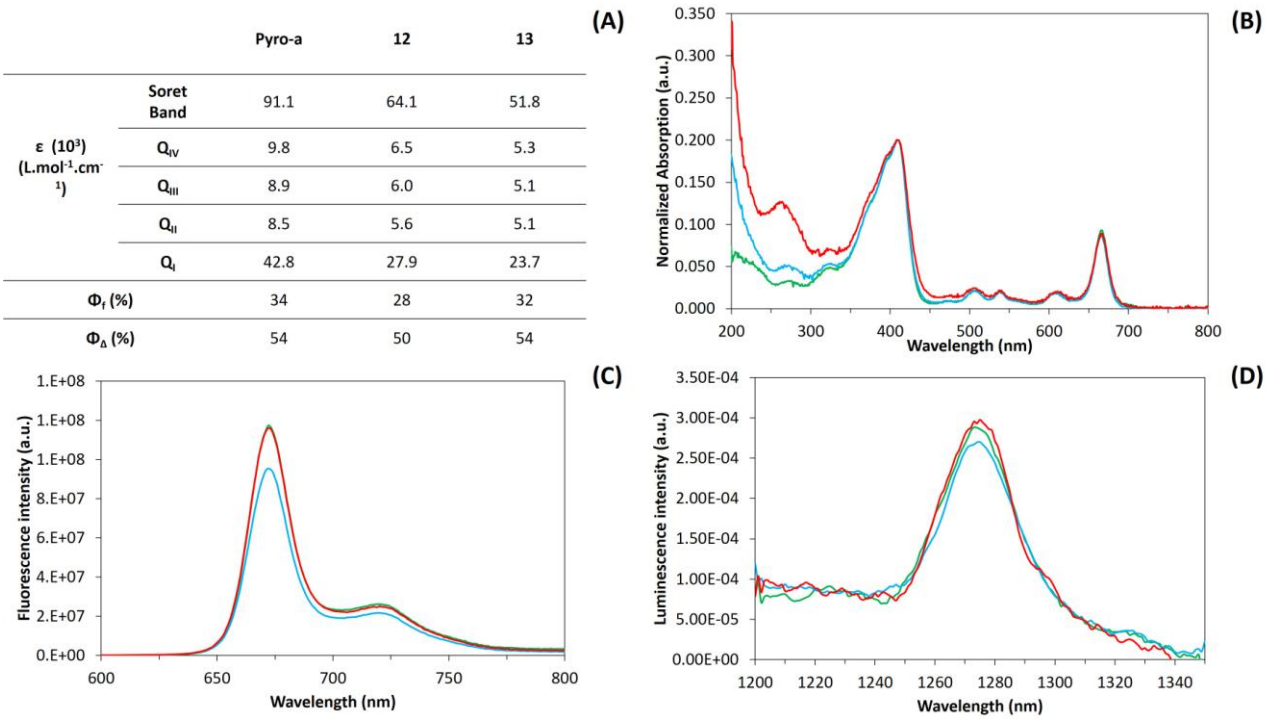

Figure 5. Photophysical properties of compounds with **Pyro-a** in methanol: (A) Absorption coefficient, Φ_f and Φ_Δ (B) Normalized UV-Visible Absorption spectra, (C) Fluorescence emission spectra (λ_{exc} = 410 nm) and (D) $^1O_2$ emission spectra (λ_{exc} = 410 nm) of **Pyro-a**, **12** and **13**. Legend: (—) **Pyro-a**, (—) **12** and (—) **13**.

Photobleaching studies

The stability of **Pyro-a, 12** and **13** under light illumination (668 nm, 10 $mW.cm^{-2}$) in methanol was studied to check the non-photobleaching of the PS over time. The Φ_f was evaluated every 5 min and a significant stability was observed for all the compounds (Figure 6). Moreover, we could observe that Φ_Δ was the same at the beginning and at the end of the illumination.

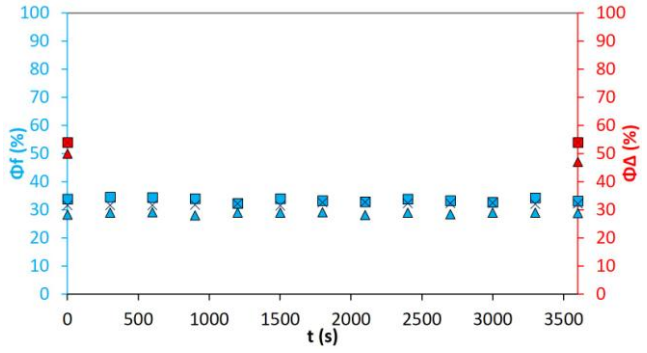

Figure 6. Evolution of Φ_f and Φ_Δ quantum yields of compounds **Pyro-a**, **12** and **13** under light irradiation (668 nm, 10 $mW.cm^{-2}$) over time. Legend: (□) **Pyro-a**, (△) **12**, (×) **13**.

Photolability studies

Scheme 4 showed the radicals production from the alk used in our model. To evaluate the effective homolysis of our compounds, we followed the generation of SG1 radical by Electron paramagnetic resonance (EPR) spectroscopy. A high stability of this radical was observed after more than 1 hour of irradiation with a decrease of intensity from 100% to 93% (data not shown).

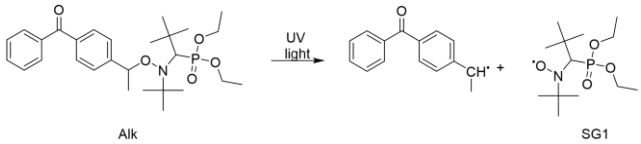

Scheme 4. Alk homolysis under UV light irradiation.

First, we opted to evaluate the influence of **Alk** concentration and oxygenation of the solution on the SG1 generation though spin-trapping investigations upon UVA-light illumination (λ = 365nm) of **Alk**. We used, as reference conditions, a 300 µM solution of **Alk** in methanol under normal conditions of oxygenation and illumination (see Material and Methods section). While doing so, EPR fingerprint of the **Alk** was detected. It consisted of 6 lines of equal intensity arising from the coupling between the single unpaired electron and both ^{31}P and ^{14}N nuclear spin of ½ and 1 respectively (hyperfine coupling values are given in Supporting Information).[19] From the very first seconds of illumination a fast production of SG1 was observed reaching a maximum EPR intensity after ca. 75 s of illumination. After this, a sharp decline of the intensity was observed (Figure 7A). The marked change in the evolution of the EPR intensity is also referred to as turnover between the radical generation (or spin adduct) and their reduction. The illumination of **Alk** at different concentration exhibited a linear dependence of the initial rate of SG1 production (Table 1) together with the **Alk** concentration. This trend was accompanied with a shift of the turnover towards higher illumination time (Figure 7A), yet such turn-

over was observed whatever was the **Alk** concentration. Similar investigations were performed on the compounds **9** and **13** (Figure 7B and 7C, respectively). Doubling the compounds concentrations were not sufficient here to double the corresponding initial rates while the presence of a well-defined turnover was also detected. The major difference was the time of illumination necessary to reach the turnover. Indeed, if the kinetics were comparable for the **Alk** alone and the compound **9**, the kinetic was significantly longer for the compound **13** which may be due to the presence of the PS. Considering the significant UV light absorption of PS, this latter may compete with the **Alk**, sharing the amount of photons received and increasing the time to reach the maximal quantity of nitroxide. However, some unexpected kinetic effect may account for these observations (vide infra).

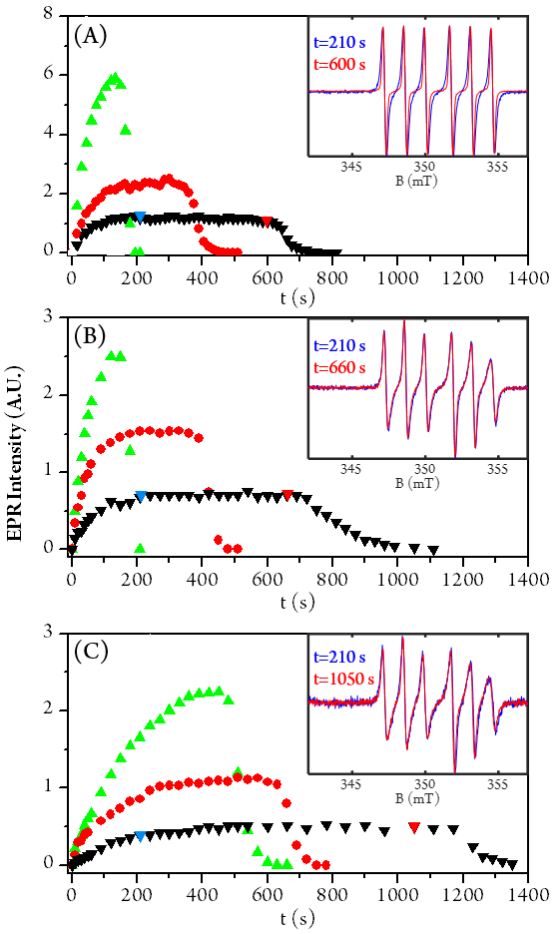

Figure 7. EPR intensity of radical generated after different irradiation time at room temperature for **Alk** (A), **9** (B) and **13** (C) at different concentrations in methanol. Inset: EPR spectra, normalized by their peak to peak intensity, of SG1 of the solution at 75 µM at the beginning of the plateau (blue) and at the end of the plateau (red). Legend: (▲) 300 µM, (●) 150 µM and (▼) 75 µM.

Worthy of note, EPR spectra of **Alk** sharpen upon irradiation (Figure 7A, inset), pointing to a decrease in O_2 concentration within the organic solvent.[20] Interestingly this effect wasn't observed neither for **9** nor **13**. The utmost importance of $^3O_2$ for the formation of radicals after irradiation of **Alk** was even strengthened by degassing the alk solution by mean of soft Argon bubbling (*ca.* 5 mL/min) prior to EPR investigations. In such hypoxic conditions, close to no SG1 was observed (Figure 8A). Identical approach was performed on both **9** and **13** compounds yet stackable kinetics were obtained regardless of the oxygenation conditions (Figure 8B and 8C). The absence of difference in Figure 8B and 8C is due to the presence of peptide and PS which play the role of alkyl radical scavengers. Indeed, in Figure 8A, a large amount of nitroxide is observed because alkyl radicals are scavenged by $^3O_2$ and back reaction is suppressed (S1) whereas in absence of $^3O_2$ back reaction occurs impeding the growth of nitroxide.

Table 1. Initial production rate (k) of radical and UV exposition time until reaching the turnover ($t_{turnover}$) for compound Alk, 9 and 13 at different concentrations in methanol.

Compound	k (A.U.)	$t_{Turnover}$ (s)
Alk (75 µM)	0.017 ± 0.001	630
Alk (150 µM)	0.031 ± 0.002	345
Alk (300 µM)	0.088 ± 0.005	135
9 (75 µM)	0.009 ± 0.001	720
9 (150 µM)	0.025 ± 0.002	390
9 (300 µM)	0.039 ± 0.002	150
13 (75 µM)	0.0031 ± 0.0005	1170
13 (150 µM)	0.011 ± 0.001	630
13 (300 µM)	0.014 ± 0.001	450

The SG1 reduction together with the potential consumption of $^3O_2$ is in favour of the photo-induced formation of radical intermediates. To validate such hypothesis a spin-trapping investigation was performed, using 5-(Diethoxyphosphoryl)-5-methyl-1-pyrroline-N-oxide (DEPMPO) to trap unstable reactive species too short-lived to be observed in our experimental conditions.[21] Indeed, the reaction between DEPMPO and targeted radical led to the formation of a more stable spin-adduct which could hence be detected by EPR spectroscopy (Scheme 5).

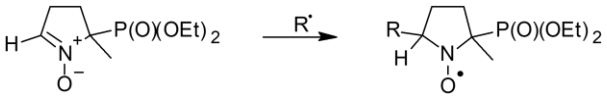

Scheme 5. Reaction between DEPMPO (EPR silent) and a short-lived radical leading to its corresponding spin adduct (EPR active).

As for SG1, DEPMPO spin-adducts exhibited the coupling between ^{31}P and ^{14}N and the unpaired electron, yet with an additional ^1H having a nuclear spin of ½. Consequently, EPR spectra of DEPMPO can have up to 12 lines. Noteworthy, the hyperfine coupling constants (*hfccs*) related to the hyperfine interaction within the adducts were characteristic of the nature of the trapped adduct, potentially allowing their identification (*e.g.* carbon- or oxygen-centred radical) (Figure 9A).[22]

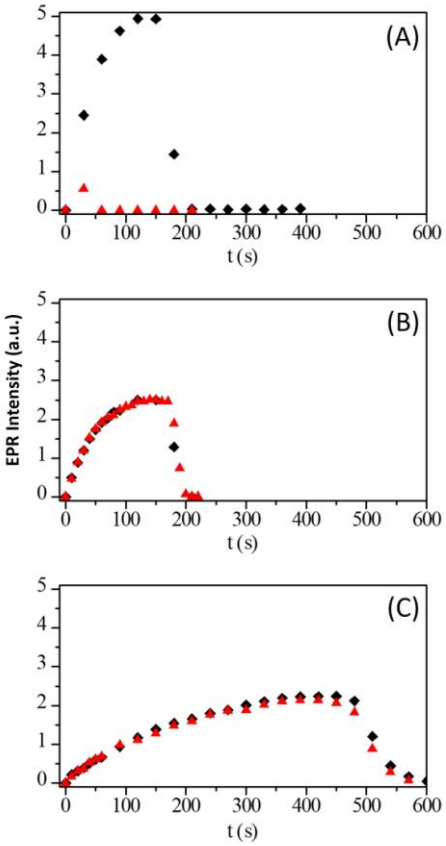

Figure 8. EPR intensity of radical generated after different irradiation time for **Alk** (A), **9** (B) and **13** (C) at 300 µM in methanol with (♦) or without (▲) oxygen.

In presence of DEPMPO, a better stability of the radical SG1 generated over illumination time was observed in both oxygenated and degassed conditions: a break was still present at significantly longer illumination time and the corresponding signal decay was significantly slowed down (Figure 9B and 9C). Quite possibly, the spin-trap shielded the SG1 nitroxide site from potential reduction due to radical intermediates. Indeed, three distinct radical species were detected and identified. Based on the obtained hyperfine interactions, the first two radicals (herein referred as to rad1 and rad2) were identified as oxygenated radicals while the latter one (denoted as rad3) pointed towards carbon centred radical (See Supporting Information).

For the compound **9** (Figure 9B and 9C), a plateau was reached pointing to the high stability of the photogenerated nitroxide radical (SG1-peptide). For a methanol solution of **9** at 300 µM, a plateau around 500 seconds was which remained stable after 1 hour of illumination and that in both conditions of oxygenation. In these conditions, three distinct spin-adducts were also observed (see Supporting Information). This high stability of the nitroxide radical generated could be explained by a protecting effect due to the peptide.

Interestingly enough, for the compound **13** (Figure 9B and 9C), the same trend as for **Alk** alone was observed with a slower decay of the nitroxide signal in normal conditions of oxygenation. The generation of the same radicals as for **9** was also observed (see Supporting Information). This difference between the kinetics of compounds **9** and **13** might be explained by the fact that the introduction of the PS, a sterically large group, changed the structure of the peptide and changed the protective effect observed in its absence.

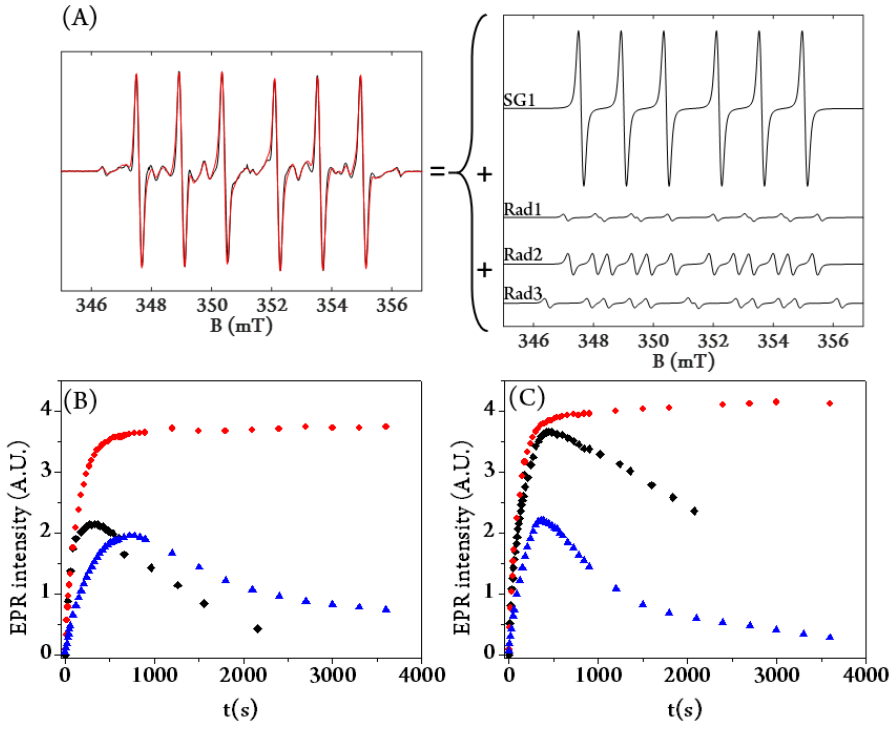

Figure 9. (A) Left: Simulation (red) and experimental (black) spectra of alk in presence of 10 mM of DEPMPO after 960 s of irradiation. Right: simulation of EPR spectra of SG1, Rad1, Rad2 and Rad3. Simulation parameters are given in Supplementary information. (B) and (C) Evolution of radical generation after illumination of **Alk**, **9** and **13** over time in solution in

MeOH at 300 µM in presence of 10 mM of DEPMPO in (B) oxygenated solution and (C) degassed solution. Legend: Radicals formed by illumination of: (♦) **Alk**, (●) **9** and (▲) **13**.

The reduction of the nitroxide radical signal highlighted its strong reactivity with the surrounding environment and although there was competition between **Alk** and PS, the generation of nitroxide radicals was far from being blocked. This is very interesting for future biological applications for the destruction of cancer cells.

Affinity studies

The affinity of **9**, **12** and **13** to neuropilin-1 was evaluated by competitive ligand binding assay in comparison with the peptide KDKPPR alone. The binding of **12** and **13** to NRP-1 showed a better specificity than the peptide alone or **9** probably due to hydrophobic interactions enhanced by **Pyro-a** and steric interactions stabilizing the 3D conformation of the peptide (Figure 10). The affinity of **13** to NRP-1 (IC_{50} of 0.46± 1 µM) was relatively encouraging to envisage an evaluation of this new multimodal therapeutic approach on *in vivo* models of tumors expressing NRP-1.

(A)

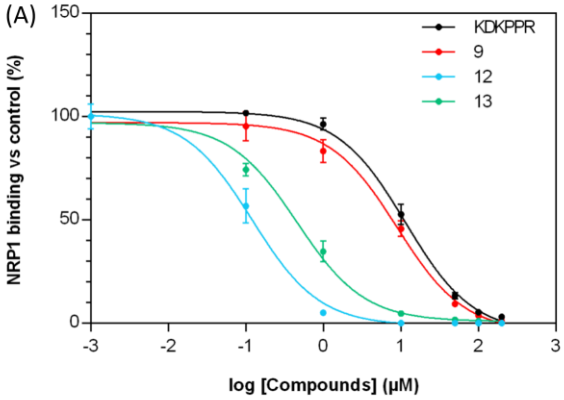

(B)

Compounds	IC50 (µM)
KDKPPR	11.5 ± 1
9	9.0 ± 1
12	0.12 ± 1
13	0.46 ± 1

Figure 10. (A) Affinity of **9**, **12** and **13** to NRP-1 evaluated by Binding Ligand Assay. (B) IC_{50} values of compounds estimated from affinity fitting curves.

CONCLUSION

Herein, we established the proof of concept that we can combine three entities, with their own properties, a PS, an alk and a peptide without any perturbations of their properties to overcome two major barriers of PDT. We report the effective synthesis of this innovative trimodal platform using SPPS with acceptable yield and high purities. The photophysical properties (quantum yields of fluorescence and $^1O_2$) of **Pyro-a** were maintained even coupled with peptide and the alk. The peptide KDKPPR still targeted NRP-1 after the coupling of **Pyro-a** and/or alk, even with a better affinity. The illumination of alk alone or coupled to the peptide or the PS led to the formation of radicals.

Concerning the photolability property of alks, compounds **9** and **13** presented two different kinetics. As an explanation, it might be suggested that the introduction of the bulky Pyro-a induced a change in the conformation of the peptide that lost its protective effect. This could be confirmed by the affinity studies where we can observe a better affinity for peptides coupling with **Pyro-a** than the peptide coupling only with (*RS/SR*)-**6.**

Although established, this proof of concept does not currently allow *in vitro* and *in vivo* applications due to the use of UV light for alk homolysis. We have to confirm our concept *in vitro* by developing others models of alk homolysable at higher wavelength.

MATERIALS AND METHODS

Synthesis of compounds

Chemicals

All commercially chemicals were used without further purifications. (3S-trans)-9-ethenyl-14-ethyl-4,8,13,18-tetramethyl-20-oxo-3-phorbinepropanoic acid (pyropheophorbide a, Pyro-a) was purchased from BOC Sciences (Shirley, NY, USA). The Benzotriazole-1-yl-oxy-tris-pyrrolidino-phosphonium hexafluorophosphate (PyBOP) was purchased from Merck (Darmstadt, Germany). The Fmoc-Arg(Pbf)-Wang resin, 9-fluorenyl-methoxy-carbonyl (Fmoc)-aminoacid-OH and *N,N,N′,N′*-Tetramethyl-O-(1H-benzotriazol-1-yl)uronium hexafluorophosphate) (HBTU) were purchased from Iris Biotech GmbH (Marktredwitz, Germany). The Fmoc-Lys-OH hydrochloride, N-hydroxysuccinimide (NHS), *N*-Ethyl-*N′*-(3-dimethylaminopropyl)carbodiimide hydrochloride (EDCI), acetic anhydride and trifluoroacetic acid (TFA) were purchased from Sigma-Aldrich (St Louis, MO, USA). The *N*-methylmorpholine (NMM), *N*-methylpyrrolidinone (NMP), *N,N*-Diisopropylethylamine (DIPEA) and triisopropylsilane (TIPS) were purchased from Alfa Aesar (Haverhill, MA, USA). Piperidine was purchased from Acros Organics. Ultrapure water (Milli-Q, ρ >18 MΩ·cm) was used for the aqueous solution preparation.

Instruments

Analytical thin layer chromatographies (TLC) were performed using Merck Kieselgel 60 F254 plates; spots were detected after UV light illumination and a phosphomolybdic acid solution in EtOH as a stain revealed by heating. Purifications of **2**, (*RR/SS*)-**4**, (*RS/SR*)-**4**, (*RS/SR*)-**5** and (*RS/SR*)-**6** were done on a Reveleris® X2 flash chromatography system (BUCHI, Switzerland) on Merck Kieselgel 60 (230-400 mesh). The synthesis of **2**, (*RR/SS*)-**4,** (*RS/SR*)-**4**, (*RS/SR*)-**5** and (*RS/SR*)-**6** were realized under anhydrous conditions and an inert atmosphere of argon and, except where stated, using dried apparatus and employing standard techniques for handling air-sensitive materials.

The peptides were synthesized with an automated ResPepXL peptide synthesizer (Intavis AG, Bioanalytical Instruments). The compounds were purified using Shimadzu LC-10ATvp, column Agilent Pursuit C18, 5 mm column (5 µm, 150 × 21.2 mm) equipped by an UV photodiode array detector (Varian Prostar 335-190-950 nm) and a spectrofluometric detector (Shimadzu RF-10A_{XL}-

200-650 nm). The UV detection was performed at 415 and 260 nm. Fluorescence detection at 650 nm was realized after an excitation at 415 nm. The analysis by HPLC were performed with the same equipment but with a column Agilent Pursuit 5 C18 (5 µm, 150 × 4.6 mm).

^{1}H, ^{13}C, and ^{31}P NMR spectra of **2**, (*RR/SS)*-**4**, (*RS/SR)*-**4**, (*RS/SR)*-**5** and (*RS/SR)*-**6** were recorded in $CDCl_3$ on a 300 or 400 MHz spectrometer at Marseille and ^{1}H, COSY and TOCSY NMR spectra of **9**, **12** and **13** were recorded in DMSO-d_6 solvent at room temperature (T = 298 K) on a BRUKER AVANCE spectrometer at 300 MHz at Nancy. Chemical shifts (δ) are given in parts per million (ppm) and using residual non- deuterated solvents as the internal reference for ^{1}H and ^{13}C-NMR spectra, and as an internal capillary filled with 85% H_3PO_4 for ^{31}P-NMR spectra for **2**, (*RR/SS)*-**4**, (*RS/SR)*-**4**, (*RS/SR)*-**5** and (*RS/SR)*-**6** and using DMSO residual peak (δ = 2.5 ppm) as internal reference for **9**, **12** and **13**. Coupling constants (J) are given in hertz (Hz) and multiplicities are reported as follow: s = singlet, d = doublet, t = triplet, q = quadruplet, m = multiplet and br = broad.

High-resolution mass spectra (HR-MS) of **2**, (*RR/SS)*-**4**, (*RS/SR)*-**4**, (*RS/SR)*-**5** and (*RS/SR)*-**6** were recorded on a SYNAPT G2 HDMS (Waters) spectrometer equipped with a pneumatically assisted atmospheric pressure ionization source (API). Positive mode electro- spray ionization was used on samples: electrospray voltage (ISV): 2800 V; opening voltage (OR): 20 V; nebulizer gas pressure (nitrogen): 800 L.h^{-1}. Electron spray ionization mass spectra (ESI-MS) of compounds **9**, **12** and **13** were recorded on a Brucker MicroTof-Q HR spectrometer in the "Service commun de Spectrométrie de Masse", Faculté des Sciences et Technologies (Vandoeuvre-lès-Nancy, France).

Alcoxyamine synthesis

Compound **2** has been synthetized by a reported procedure[23] (see SI) by using 10 mol% of azobisisobutyronitrile instead of 1 mol % of benzoyl peroxide.

The new compounds 4, 5, 6 have been prepared according to a reported procedure[24] (see SI).

Solid phase peptide synthesis (SPPS)

The peptides K(Boc)D(OtBu)K(Boc)PPR(Pbf)-Wang resin **8** and D(OtBu)K(Boc)PPR(Pbf)-Wang resin **10** were first synthesized using the automated ResPepXL peptide synthesizer, with a Fmoc/*t*Bu methodology. The side chains of arginine, lysine and aspartic acid were respectively protected by Pbf, OtBu and Boc groups. We used a Fmoc-Arg(Pbf)-Wang resin swelled in CH_2Cl_2. To remove the Fmoc group we used piperidine (20% in DMF). This step was performed two times, a first during 4 min and a second during 7 min. Then the next amino acid was grafted by adding an excess of Fmoc-aminoacid-OH (6 eq), HBTU (5 eq), NMP (3 eq) and NMM (10 eq) in DMF. This step was repeated two times for 18 min. A last step of capping, using a solution of acetic anhydride (5% in DMF), was performed for 5 min, to trap all functions that did not react. Deprotection, coupling and capping steps were repeated until the end of the synthesis of the peptide.

Alk-KDKPPR, ***9.***

After Fmoc deprotection, the reaction between *(RS/SR)*-**6** (1.5 eq) and peptide K(Boc)D(OtBu)K(Boc)PPR(Pbf)-Wang resin **8** was performed in presence of PyBOP (3 eq) and DIPEA (3 eq) in DMF, and the solution was stirred for 12 h. The resin was dried under vacuum and then cleaved (with full deprotection of lateral chains) using TFA/TIPS/water (92.5/2.5/5%) for 2 h. The acidic resin was filtered and washed with CH_2Cl_2 and EtOH. The filtrate was dried under vacuum and the compound was precipitated in ether by centrifugation. The final product was further purified by preparative HPLC using acetonitrile/water (0.1% TFA; 10/90) to 100% acetonitrile gradient in 25 min at a flow of 12 mL.min^{-1}. *R*t =13.2 min. **9** was isolated as a white powder with a yield of 27% (8.60 mg) and a HPLC purity of 95%.

K(Pyro)DKPPR, ***12.***

After Fmoc deprotection, the reaction between **Fmoc-K(Pyro-a)** (1.5 eq) and peptide D(OtBu)K(Boc)PPR(Pbf)-Wang resin **10** was performed with HBTU (3 eq), NMP (3 eq) and NMM (9 eq) in DMF and the mixture was stirred for 12h to conduct to the Fmoc and lateral protected compound **11**. The final Fmoc protection was removed using piperidine. The resin was dried under vacuum and then cleaved (with full deprotection of lateral chains) using TFA/TIPS/water (92.5/2.5/5%) for 2 h. The acidic resin was filtered and washed with CH_2Cl_2 and EtOH. The filtrate was dried under vacuum and the compound was precipitated in ether by centrifugation. The final product was purified by preparative HPLC using acetonitrile/water (0.1% TFA; 10/90) to 100% acetonitrile gradient in 15 min, followed by isocratic acetonitrile for 10 min at a flow of 12 mL.min^{-1}. *R*t =12.9 min. **12** was isolated as a dark green powder with a yield of 25% (15.57 mg) and a HPLC purity of 100%.

Alk-K(Pyro-a)DKPPR, ***13.***

Following the synthesis of the product **11** on resin, the coupling reaction with *(RS/SR)*-**6** (1.5 eq) was performed in presence of PyBOP (3 eq) and DIPEA (3 eq) in DMF, and the reaction mixture was stirred for 12 h. The resin obtained was dried under vacuum and then cleaved (with full deprotection of lateral chains) using TFA/TIPS/water (92.5/2.5/5%) for 2 h then filtered and washed with CH_2Cl_2 and EtOH. The filtrate was dried under vacuum and the compound was precipitated in ether by centrifugation. The final product was purified using an Armen SPOT Prep system (high pressure, preparative liquid chromatography) using a column, using acetonitrile/water (0.1% TFA; 10/90) to 100% acetonitrile gradient in 15 min, followed by isocratic acetonitrile for 10 min at a flow of 15 mL.min^{-1}. *R*t =18.3 min. **13** was isolated as a dark green powder with a yield of 19% (8.25 mg) and a HPLC purity of 98%.

Photophysical properties

The set ups and the methods have been already described in a previous study.[25]

Photobleaching of Pyropheophorbide-a

The studies of photobleaching were performed with a red laser (λ = 668 nm and P = 10 mW.cm^{-2}). The solutions of **Pyro-a**, **12** and **13** were prepared in order to have an absorbance around 0.2 to follow the evolution of fluorescence and singlet oxygen emission. The solutions were irradiated and the photophysical properties of each com-

pound were evaluated at different times of irradiation: 0, 5, 10, 15, 20, 25, 30, 35, 40, 45, 50, 55 and 60 min with the same instruments as described below.

Homolysis of Alk

EPR spectra were recorded as previously described[26] except the microwave power was at 4.5 mW, modulation amplitude et 2 G, a sweep time of 30 s for a single scan and 25 µL capillaries (Hirschmann) were used. 5-(Diethoxyphosphoryl)-5-methyl-1-pyrroline-N-oxide (DEPMPO) was synthesized as reported in the literature.[21] DEPMPO was stored in a stock solution at 0.5 M in acetonitrile. The intensity of the EPR spectra was obtained by calculating the double integral of the EPR spectra. In case of multiple component spectra, spectra were simulated using Easyspin toolbox under Matlab (Mathworks) environment.[27] The parameters used for simulation are presented in Supporting information table S2. The double integral of each component of the simulated spectra was used to get the intensity of each component. Initial rates were calculated by performing a linear fit on the 4 first points of the kinetics using OriginPro, version 8, fitting tool.

Affinity tests

Competitive binding to recombinant NRP-1 protein

The binding of compounds for NRP-1 protein was evaluated in terms of the half maximal inhibitory concentration (IC_{50} values) through a competitive assay as previously described[28]. (See SI)

ASSOCIATED CONTENT

Supporting Information. "This material is available free of charge via the Internet at http://pubs.acs.org." S1. Synthesis and analytical characterizations of **2**, (*RR/SS*)-**4**, (*RS/SR*)-**4**, (*RS/SR*)-**5** and (*RS/SR*)-**6**, **9**, **12** and **13**. S2. Photophysical properties. S3. Homolysis studies. S4. Competitive binding to recombinant NRP-1 protein.

AUTHOR INFORMATION

Corresponding Author

* celine.frochot@univ-lorraine.fr; Tel.: +33-3-72-74-37-80; g.audran@univ-amu.fr; Tel.: +33-4-91-28-88-62

Author Contributions

The manuscript was written through contributions of all authors. All authors have given approval to the final version of the manuscript.

Funding Sources

This research received no external funding.

ACKNOWLEDGMENT

We gratefully acknowledge François Courtier, Marc Basler and Dr. David Martel (Institut Charles Sadron, Strasbourg, France) for designing & building of the illumination chamber. The authors thank the French Ministry of Research and the REseauNAtional de Rpeinter-Disciplinaire (RENARD, Fédération IR-RPE CNRS #3443). Dr. Elena Gimenez-Arnau (Dermatochemistry Laboratory, University of Strasbourg, France) is acknowledged for providing us with DEPMPO. We also aknowledge André Merlin, LERMAB, CNRS, Université de Lorraine for his help with the RPE experiments, Olivier Fabre, LCPM, CNRS, Université de Lorraine, for the NMR experiments and Serge Mordon, ONCOTHAI, INSERM, Université de Lille, CHU for the loan of the lighting equipment.

ABBREVIATIONS

Alk, alkoxyamine; AMD, age-related macular degeneration; DCM, dichloromethane; DIPEA, Diisopropylethylamine; DMF, diméthylformamide; DMP, Dess–Martin periodinane; DO, optical density; EDCI, *N*-Ethyl-*N*′-(3-dimethylaminopropyl)carbodiimide hydrochloride; EPR, Electronic paramagnetic resonance; HBTU, *N,N,N′,N′*-Tetramethyl-O-(1H-benzotriazol-1-yl)uronium hexafluorophosphate); HO•, hydroxyl radical; HPLC, high performance liquid chromatography; HR-MS, high-resolution mass spectrometry; NBS, *N*-bromosuccinimide; NHS, *N*-hydroxysuccinimide; NMM, *N*-methylmorpholine; NMP, Nitroxide Mediated Polymerization; NMR, nuclear magnetic resonance; NO, nitric oxide; NRP-1, neuropilin-1; O_2, molecular oxygen; $^1O_2$, singlet oxygen; $O_2^{-\bullet}$, superoxide anion; PDT, photodynamic therapy; pip, piperidine; PS, photosensitizer; PTT, photothermal therapy; PyBOP, Benzotriazole-1-yl-oxy-tris-pyrrolidino-phosphonium hexafluorophosphate; Pyro-a, pyropheophorbide-a; ROS, reactive oxygen species; TFA, trifluoroacetic acid; THF, tetrahydrofuran; TIPS, triisopropylethylamine; TLC, thin layer chromatography; UV, ultra-violet; VEGF, vascular endothelial growth factor.

REFERENCES

(1) Hamblin, M. *Advances in Photodynamic Therapy: Basic, Translational, and Clinical*; Artech House, 2008.

(2) See, K. L.; Forbes, I. J.; Betts, W. H. Oxygen Dependency of Photocytotoxicity with Haematoporphyrin Derivative. *Photochemistry and Photobiology* **1984**, *39* (5), 631–634. https://doi.org/10.1111/j.1751-1097.1984.tb03902.x.

(3) Larue; Myrzakhmetov; Ben-Mihoub; Moussaron; Thomas; Arnoux; Baros; Vanderesse; Acherar; Frochot. Fighting Hypoxia to Improve PDT. *Pharmaceuticals* **2019**, *12* (4), 163. https://doi.org/10.3390/ph12040163.

(4) Kovtun, G. A.; Aleksandrov, A. L.; Golubev, V. A. Interaction of Peroxide Radicals with Esters of Hydroxylamines. *Russ Chem Bull* **1974**, *23* (10), 2115–2121. https://doi.org/10.1007/BF00921266.

(5) Bertin, D.; Gigmes, D.; Marque, S. R. A.; Tordo, P. Kinetic Subtleties of Nitroxide Mediated Polymerization. *Chem. Soc. Rev.* **2011**, *40* (5), 2189. https://doi.org/10.1039/c0cs00110d.

(6) Bagryanskaya, E. G.; Marque, S. R. A. Chapter 2:Kinetic Aspects of Nitroxide Mediated Polymerization. In *Nitroxide Mediated Polymerization*; 2015; pp 45–113. https://doi.org/10.1039/9781782622635-00045.

(7) Moncelet, D.; Voisin, P.; Koonjoo, N.; Bouchaud, V.; Massot, P.; Parzy, E.; Audran, G.; Franconi, J.-M.; Thiaudière, E.; Marque, S. R. A.; Brémond, P.; Mellet, P. Alkoxyamines: Toward a New Family of Theranostic Agents against Cancer. *Molecular Pharmaceutics* **2014**, *11* (7), 2412–2419. https://doi.org/10.1021/mp5001394.

(8) Yamasaki, T.; Buric, D.; Chacon, C.; Audran, G.; Braguer, D.; Marque, S. R. A.; Carré, M.; Brémond, P. Chemical Modifications of Imidazole-Containing Alkoxyamines Increase C–ON Bond Homolysis Rate: Effects on Their Cytotoxic Properties in Glioblastoma Cells. *Bioorganic & Medicinal Chemistry* **2019**, *27* (10), 1942–1951. https://doi.org/10.1016/j.bmc.2019.03.029.

(9) Popova, N. A.; Sysoeva, G. M.; Nikolin, V. P.; Kaledin, V. I.; Tretyakov, E. V.; Edeeva, M. V.; Balakhnin, S. M.; Lushnikova, E. L.; Audran, G.; Mark, S. Comparative Study of Toxicity of Alkoxyamines In Vitro and In Vivo. *Bulletin*

of Experimental Biology and Medicine **2017**, *164* (1), 49–53. https://doi.org/10.1007/s10517-017-3924-6.

(10) Benachour, H.; Frochot, C.; Vanderesse, R.; Guillemin, F.; Barberi-Heyob, M. Targeting Strategies in Photodynamic Therapy for Cancers Treatment. In *Brain Cancer, Tumor Targeting and Cervical Cancer*; Salvatti, E., Ed.; Novapublishers, 2011; pp 1–38.

(11) Krishnamurthy, S.; Witmer, P. Optimal Light Dose for Interstitial Photodynamic Therapy in Treatment for Malignant Brain Tumors. *Lasers Surg. Med.* **2000**, *27*, 224–234. https://doi.org/10.1002/1096-9101(2000)27:3<224::AID-LSM4>3.0.CO;2-%23.

(12) Tirand, L.; Frochot, C.; Vanderesse, R.; Thomas, N.; Trinquet, E.; Pinel, S.; Viriot, M.-L.; Guillemin, F.; Barberi-Heyob, M. A Peptide Competing with VEGF165 Binding on Neuropilin-1 Mediates Targeting of a Chlorin-Type Photosensitizer and Potentiates Its Photodynamic Activity in Human Endothelial Cells. *Journal of Controlled Release* **2006**, *111* (1–2), 153–164. https://doi.org/10.1016/j.jconrel.2005.11.017.

(13) Corbin, T. F.; Hahn, R. C.; Shechter, H. Cyclopropylbenzene. *Organic Syntheses* **2003**, 30–30. https://doi.org/10.1002/0471264180.os044.10.

(14) Audran, G.; Bikanga, R.; Brémond, P.; Edeleva, M.; Joly, J.-P.; Marque, S. R. A.; Nkolo, P.; Roubaud, V. How Intramolecular Hydrogen Bonding (IHB) Controls the C–ON Bond Homolysis in Alkoxyamines. *Org. Biomol. Chem.* **2017**, *15* (39), 8425–8439. https://doi.org/10.1039/C7OB02223A.

(15) Home - The Cambridge Crystallographic Data Centre (CCDC) https://www.ccdc.cam.ac.uk/ (accessed Oct 1, 2019).

(16) Dess, D. B.; Martin, J. C. A Useful 12-I-5 Triacetoxyperiodinane (the Dess-Martin Periodinane) for the Selective Oxidation of Primary or Secondary Alcohols and a Variety of Related 12-I-5 Species. *J. Am. Chem. Soc.* **1991**, *113* (19), 7277–7287. https://doi.org/10.1021/ja00019a027.

(17) Bal, B. S.; Childers, W. E.; Pinnick, H. W. Oxidation of α,β-Un Saturated Aldehydes. *Tetrahedron* **1981**, *37* (11), 2091–2096. https://doi.org/10.1016/S0040-4020(01)97963-3.

(18) Youssef, Z.; Yesmurzayeva, N.; Larue, L.; Jouan-Hureaux, V.; Colombeau, L.; Arnoux, P.; Acherar, S.; Vanderesse, R.; Frochot, C. New Targeted Gold Nanorods for the Treatment of Glioblastoma by Photodynamic Therapy. *Journal of Clinical Medicine* **2019**, *8* (12), 2205. https://doi.org/10.3390/jcm8122205.

(19) Bertrand, P. Hyperfine Structure of a Spectrum in the Isotropic Regime. In *Electron Paramagnetic Resonance Spectroscopy: Fundamentals*; Bertrand, P., Ed.; Springer International Publishing: Cham, 2020; pp 31–59. https://doi.org/10.1007/978-3-030-39663-3_2.

(20) Pryor, W. A. *Bio-Assays for Oxidative Stress Status*; Elsevier, 2012.

(21) Barbati, S.; Clément, J. L.; Olive, G.; Roubaud, V.; Tuccio, B.; Tordo, P. 31P Labeled Cyclic Nitrones: A New Class of Spin Traps for Free Radicals in Biological Milieu. In *Free Radicals in Biology and Environment.*; Nato Science Partnership Subseries: 3; Springer Netherlands, 1997; pp 39–47.

(22) Lauricella, R.; Tuccio, B. Detection and Characterisation of Free Radicals After Spin Trapping. In *Electron Paramagnetic Resonance Spectroscopy: Applications*; Bertrand, P., Ed.; Springer International Publishing: Cham, 2020; pp 51–82. https://doi.org/10.1007/978-3-030-39668-8_3.

(23) Cauble, D. F.; Lynch, V.; Krische, M. J. Studies on the Enantioselective Catalysis of Photochemically Promoted Transformations: "Sensitizing Receptors" as Chiral Catalysts. *J. Org. Chem.* **2003**, *68* (1), 15–21. https://doi.org/10.1021/jo020630e.

(24) Audran, G.; Brémond, P.; Marque, S. R. A.; Yamasaki, T. C–ON Bond Homolysis of Alkoxyamines, Part 11: Activation of the Nitroxyl Fragment. *J. Org. Chem.* **2016**, *81* (5), 1981–1988. https://doi.org/10.1021/acs.joc.5b02790.

(25) Stallivieri, A.; Colombeau, L.; Jetpisbayeva, G.; Moussaron, A.; Myrzakhmetov, B.; Arnoux, P.; Acherar, S.; Vanderesse, R.; Frochot, C. Folic Acid Conjugates with Photosensitizers for Cancer Targeting in Photodynamic Therapy: Synthesis and Photophysical Properties. *Bioorganic & Medicinal Chemistry* **2017**, *25* (1), 1–10. https://doi.org/10.1016/j.bmc.2016.10.004.

(26) Twardoch, M.; Messai, Y.; Vileno, B.; Hoarau, Y.; Mekki, D. E.; Felix, O.; Turek, P.; Weiss, J.; Decher, G.; Martel, D. Development of an Electron Paramagnetic Resonance Methodology for Studying the Photo-Generation of Reactive Species in Semiconductor Nano-Particle Assembled Films. *Molecular Physics* **2018**, *116* (12), 1558–1564. https://doi.org/10.1080/00268976.2018.1433882.

(27) Stoll, S.; Schweiger, A. EasySpin, a Comprehensive Software Package for Spectral Simulation and Analysis in EPR. *Journal of Magnetic Resonance* **2006**, *178* (1), 42–55. https://doi.org/10.1016/j.jmr.2005.08.013.

(28) Thomas, N.; Pernot, M.; Vanderesse, R.; Becuwe, P.; Kamarulzaman, E.; Da Silva, D.; François, A.; Frochot, C.; Guillemin, F.; Barberi-Heyob, M. Photodynamic Therapy Targeting Neuropilin-1: Interest of Pseudopeptides with Improved Stability Properties. *Biochemical Pharmacology* **2010**, *80* (2), 226–235. https://doi.org/10.1016/j.bcp.2010.03.036.

TOC

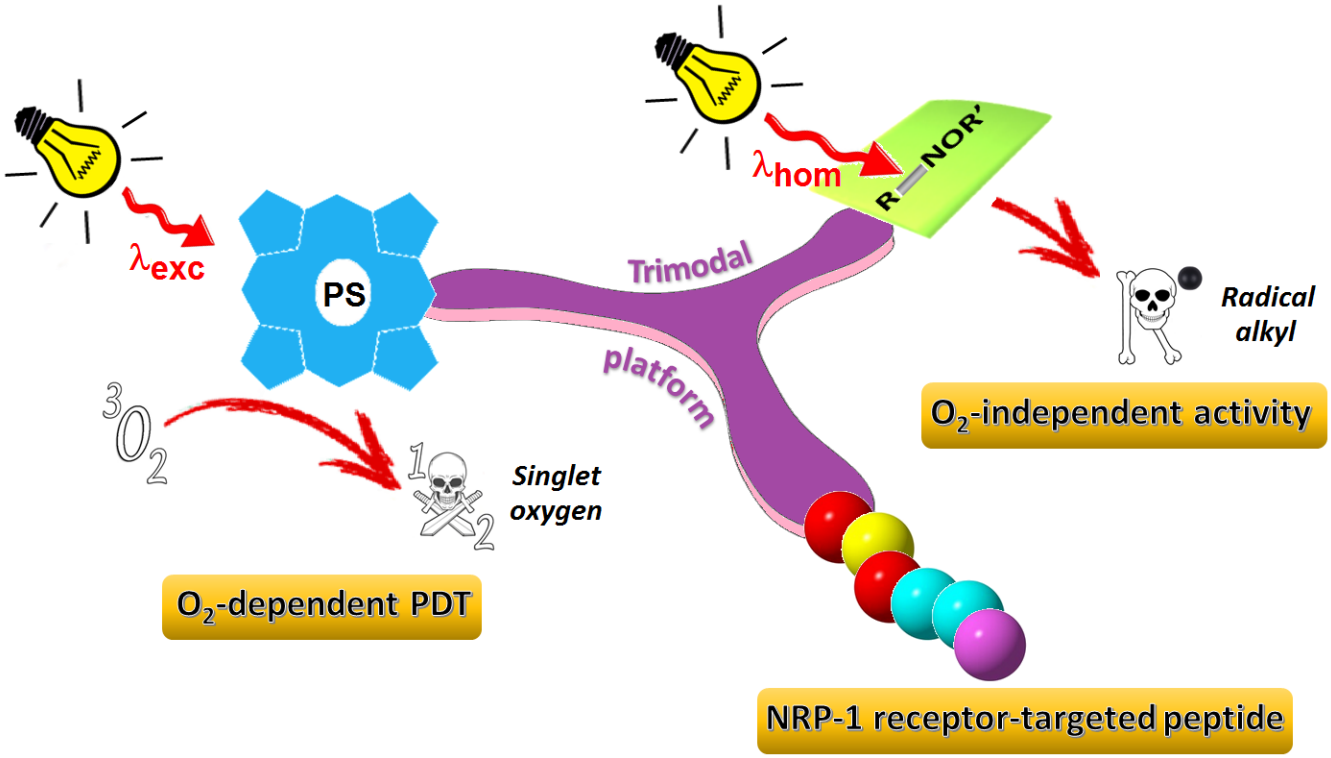
λexc
PS
Trimodal
platform
λhom
R NOR'
Radical
alkyl
O2-independent activity
3O2
1O2
Singlet
oxygen
O2-dependent PDT
NRP-1 receptor-targeted peptide